Local Fault Detection of Intershaft Bearing in Aircraft Engines

MaZhenguo

School of Power and Energy
Northwestern Polytechnical University
Xi'an City, China
e-mail: mazhenguo1983@outlook.com

Liaongfu

School of Power and Energy
Northwestern Polytechnical University
Xi'an City, China
e-mail: mazhenguo1983@outlook.com

Abstract—**Rotation speed difference domain (RSDD) frequency spectrum and RSDD envelop spectrum are presented for sake of detecting intershaft bearing with local defect. The methods are used to analyze vibration signal measured from intershaft bearing test rig. Results of the theoretical analysis show that, positions of unbalance response, misalignment response, and bearings with a stationary outer race on RSDD frequency spectrum and envelop spectrum vary with rotation speeds. As for intershaft bearing in RSDD, distances between adjacent side frequencies in frequency spectrum and positions of characteristic defect multiple frequencies in envelop spectrum keep constant under variational rotation speeds of outer race and inner race, which are called characteristic "constant distances" and "constant frequencies". The experiment of intershaft bearing with local fatigue peeling on its outer raceway indicates that the theory is verified and useful in diagnosing faults of intershaft bearing.**

Keywords-aircraft engine; intershaft bearing, fault detection, rotation speed difference domain envelope spectrum, constant frequencies, constant distances

I. INTRODUCTION

In order to reduce the weight of turbofan engine, intershaft bearing is used. Owing to high operating temperature, difficult to ensure lubrication condition, and heavy dynamic load, intershaft bearing may go wrong. Failure of intershaft bearing is dangerous to turbofan engines. So it is important to diagnose fault when the fault is an incipient failure.

Vibration signals measured by an accelerometer located at supporting-case are analyzed for condition monitoring of turbofan engine as well as intershaft bearing. But signals may also contain unbalance responses of high pressure rotor and low pressure rotor, vibration due to misalignment, and vibration due to outer-race-fixed bearings, etc. Method based on characteristic defect multiple frequencies in a rolling element bearing is suitable for outer-race-fixed bearing [1]. So, in order to find vibration caused by intershaft bearing and diagnose fault of intershaft bearing, vibration signals measured by

accelerometer must be analyzed and new method applicable to intershaft bearing has to be developed.

I. COMPONENTS AND CHARACTERISTICS OF CASING VIBRATION SIGNAL

Generally, accelerometers are mounted on casing of aero-engine to monitor vibration. Vibration caused by every part of turbofan engine may be transferred to the casing. So, vibration signal $x(t)$ measured by an accelerometer can be expressed as

$$
\begin{aligned}
x(t) = & A_{\mathrm{h}} \cos(\Omega_{\mathrm{h}} t + \beta_{\mathrm{h}}) + A_{\mathrm{l}} \cos(\Omega_{\mathrm{l}} t + \beta_{\mathrm{l}}) \\
& + \sum_{k=1}^{N} A_{\mathrm{l}k} \cos(k\Omega_{\mathrm{l}} t + \beta_{\mathrm{l}k}) \\
& + \sum_{k=1}^{S} Q_{\mathrm{hb}}(\Omega_{\mathrm{h}} F_{\mathrm{hb}} t) * h(\omega_{\mathrm{hb}k} t) \\
& + \sum_{k=1}^{T} Q_{\mathrm{lb}}(\Omega_{\mathrm{l}} F_{\mathrm{lb}} t) * h(\omega_{\mathrm{lb}k} t) \\
& + \sum_{k=1}^{R} Q_{\mathrm{interb}}(F_{\mathrm{interb}}(\Omega_{\mathrm{h}} - \Omega_{\mathrm{l}}) t) * h(\omega_{\mathrm{interb}k} t) \\
& + \ldots
\end{aligned}
\tag{1}
$$

where Ω_{h} is rotation speed of high pressure rotor, Ω_{l} is rotation speed of low pressure rotor, A_{h} and β_{h} are amplitude and phase of unbalance response of high pressure rotor, A_{l} and β_{l} are amplitude and phase of unbalance response of low pressure rotor, $A_{\mathrm{l}k}$ and $\beta_{\mathrm{l}k}$ are amplitude and phase of misalignment response of low pressure rotor, Q_{hb} is periodic pulse excitation function caused by certain element fault of high pressure rotor bearing, F_{hb} is characteristic defect multiple frequency of certain element fault of high pressure rotor bearing, h is response of bearing under unit pulse excitation, $\omega_{\mathrm{hb}k}$ is the k _th order natural frequency of high pressure rotor

bearing, Q_{lb} is periodic pulse excitation function caused by certain element fault of low pressure rotor bearing, F_{lb} is characteristic defect multiple frequency of certain element fault of low pressure rotor bearing, ω_{lbk} is the k _th order natural frequency of low pressure rotor bearing, Q_{lb} is periodic pulse excitation function caused by certain element fault of intershaft bearing, F_{interb} is characteristic defect multiple frequency of certain element fault of intershaft bearing, $\omega_{interbk}$ is the k _th order natural frequency of intershaft bearing,

Vibration signals measured from casing contain not only fault response of intershaft bearing, but also unbalance response of high pressure rotor and low pressure rotor, misalignment response of low pressure rotor, fault response of high pressure rotor and low pressure rotor bearings, accessories vibration, etc. Since the other vibrations generally are stronger than vibration caused by intershaft bearing, it is difficult to extract vibration information caused by intershaft bearing from vibration signals measured from casing.

Frequency analysis is accomplished to vibration signal $x(t)$. As the result, frequency spectrum of $x(t)$ is obtained:

$$
\begin{aligned}
X(\omega) = {} & \pi A_{h} e^{j\beta_h} \delta(\omega - \Omega_h) + \pi A_l e^{j\beta_l} \delta(\omega - \Omega_l) \\
& + \sum_{k=1}^{N} \pi A_{lk} e^{j\beta_{lk}} \delta(\omega - k\Omega_l) \\
& + \sum_{k=1}^{S} \sum_{m=-M}^{M} A_{hbk}^{(m)} \delta(\omega - \omega_{hbk} + mF_{hb}\Omega_h) \\
& + \sum_{k=1}^{T} \sum_{m=-P}^{P} A_{lbk}^{(m)} \delta(\omega - \omega_{lbk} + mF_{lb}\Omega_l) \\
& + \sum_{k=1}^{R} \sum_{m=-J}^{J} A_{interbk}^{(m)} \delta(\omega - \omega_{interbk} + mF_{interb}(\Omega_h - \Omega_l)) \\
& + ...
\end{aligned}
\tag{2}
$$

where $A_{hbk}^{(m)}$ is amplitude of the m _th order side frequency of the k _th order natural frequency of high pressure rotor bearing, $A_{lbk}^{(m)}$ and $A_{interbk}^{(m)}$ have similar meanings, δ is the unit pulse function.

Equation (2) shows that, position of every frequency caused by any fault changes along with rotation speeds of high pressure rotor and low pressure rotor. If a bearing goes wrong, periodic pulse response will be excited, and side frequencies will appear around a certain natural frequency. Distances between adjacent side frequencies will change along with rotation speeds of high pressure rotor and low pressure rotor.

Envelope analysis is accomplished to vibration signal $x(t)$. As the result, envelop signal $\hat{x}(t)$ is obtained:

$$
\begin{aligned}
\hat{x}(t) = {} & \sum_{k=1}^{M} \hat{A}_{hbk} \cos(kF_{hb}\Omega_h t + \beta_{hbk}) \\
& + \sum_{k=1}^{S} \hat{A}_{lbk} \cos(kF_{lb}\Omega_l t + \beta_{lbk}) \\
& + \sum_{k=1}^{P} \hat{A}_{interbk} \cos(kF_{interb}(\Omega_h - \Omega_l)t + \beta_{interbk}) \\
& + ...
\end{aligned}
\tag{3}
$$

where $\hat{A}_{hbk}$ and β_{hbk} are amplitude and phase of the k_th order characteristic defect multiple frequency of certain element fault of high pressure rotor bearing, $\hat{A}_{lbk}$ and β_{lbk} are amplitude and phase of the k_th order characteristic defect multiple frequency of certain element fault of low pressure rotor bearing, $\hat{A}_{interbk}$ and $\beta_{interbk}$ are amplitude and phase of the k_th order characteristic defect multiple frequency of certain element fault of intershaft bearing.

Frequency analysis is accomplished to envelop signal $\hat{x}(t)$. As the result, envelop spectrum $\hat{X}(\omega)$ is obtained:

$$
\begin{aligned}
\hat{X}(\omega) = {} & \sum_{k=1}^{M} \hat{A}_{hbk} e^{j\beta_{hbk}} \delta(\omega - kF_{hb}\Omega_h) \\
& + \sum_{k=1}^{S} \hat{A}_{lbk} e^{j\beta_{lbk}} \delta(\omega - kF_{lb}\Omega_l) \\
& + \sum_{k=1}^{P} \hat{A}_{interbk} e^{j\beta_{interbk}} \delta(\omega - kF_{interb}(\Omega_h - \Omega_l))
\end{aligned}
\tag{4}
$$

Equation (4) shows that, in envelop spectrum, frequencies caused by intershaft bearing change along with rotation speeds of high pressure rotor and low pressure rotor, which results in inconvenience of analysis.

II. FREQUENCY SPECTRUM AND ENVELOP SPECTRUM OF CASING VIBRATION SIGNAL IN ROTATION SPEED DIFFERENCE DOMAIN

Equation (1) to (4) show that, frequencies caused by intershaft bearing change along with $\Omega_h - \Omega_l$. To highlight fault information of intershaft bearing, frequency analysis will be done in RSDD.

Let $\eta = \dfrac{\Omega_l}{\Omega_h}$ and $\Delta\Omega_{hl} = \Omega_h - \Omega_l$, then

$$
\Omega_h = \frac{\Delta\Omega_{hl}}{1 - \eta}, \quad \Omega_l = \frac{\Delta\Omega_{hl}\eta}{1 - \eta} .
\tag{5}
$$

Rewriting (1),

$$x(\tau) = A_{\mathrm{h}} \cos\left(\frac{\tau}{1-\eta} + \beta_{\mathrm{h}}\right) + A_{\mathrm{l}} \cos\left(\frac{\eta\tau}{(1-\eta)} + \beta_{\mathrm{l}}\right)$$

$$+ \sum_{k=1}^{N} A_{\mathrm{l}k} \cos\left(\frac{\eta k\tau}{(1-\eta)} + \beta_{\mathrm{l}k}\right)$$

$$+ \sum_{k=1}^{S} Q_{\mathrm{hb}}\left(\frac{F_{\mathrm{hb}}\tau}{1-\eta}\right) * h\left(\frac{\omega_{\mathrm{hb}k}\tau}{\Delta\Omega_{\mathrm{hl}}}\right) \qquad , \quad (6)$$

$$+ \sum_{k=1}^{T} Q_{\mathrm{lb}}\left(\frac{\eta F_{\mathrm{lb}}\tau}{(1-\eta)}\right) * h\left(\frac{\omega_{\mathrm{lb}k}\tau}{\Delta\Omega_{\mathrm{hl}}}\right)$$

$$+ \sum_{k=1}^{R} Q_{\mathrm{interb}}\left(F_{\mathrm{interb}}\tau\right) * h\left(\frac{\omega_{\mathrm{interb}k}\tau}{\Delta\Omega_{\mathrm{hl}}}\right)$$

$$+ \ldots$$

where $\tau = \Delta\Omega_{\mathrm{hl}}t = (1-\eta)\Omega_{\mathrm{h}}t = \dfrac{(1-\eta)}{\eta}\Omega_{\mathrm{l}}t$.

Let $\omega' = \dfrac{\omega}{\Omega_{\mathrm{h}} - \Omega_{\mathrm{l}}}$, rewriting (2), RSDD frequency spectrum is obtained,

$$X(\omega') = \pi A_{\mathrm{h}} e^{j\beta_{\mathrm{h}}} \delta\left(\omega' - \frac{1}{1-\eta}\right)$$

$$+ \pi A_{\mathrm{l}} e^{j\beta_{\mathrm{l}}} \delta\left(\omega' - \frac{\eta}{1-\eta}\right)$$

$$+ \sum_{k=1}^{N} \pi A_{\mathrm{l}k} e^{j\beta_{\mathrm{l}k}} \delta\left(\omega' - \frac{k\eta}{1-\eta}\right)$$

$$+ \sum_{k=1}^{S} \sum_{m=-M}^{M} A_{\mathrm{hb}k}^{(m)} \delta\left(\omega' - \frac{\omega_{\mathrm{hb}k}}{\Delta\Omega_{\mathrm{hl}}} + \frac{mF_{\mathrm{hb}}}{1-\eta}\right) \quad , \quad (7)$$

$$+ \sum_{k=1}^{T} \sum_{m=-P}^{P} A_{\mathrm{lb}k}^{(m)} \delta\left(\omega' - \frac{\omega_{\mathrm{lb}k}}{\Delta\Omega_{\mathrm{hl}}} + \frac{\eta mF_{\mathrm{lb}}}{1-\eta}\right)$$

$$+ \sum_{k=1}^{R} \sum_{m=-J}^{J} A_{\mathrm{interb}k}^{(m)} \delta\left(\omega' - \frac{\omega_{\mathrm{interb}k}}{\Delta\Omega_{\mathrm{hl}}} + mF_{\mathrm{interb}}\right)$$

$$+ \ldots$$

Equation (7) shows that, natural frequencies ($\omega_{\mathrm{hb}k}$, $\omega_{\mathrm{lb}k}$ and $\omega_{\mathrm{interb}k}$) of bearings change its position on ω'-axis along with rotation speeds of high pressure rotor and low pressure rotor. Distances between adjacent side frequencies of outer-race-fixed bearing change along with rotation speeds of high pressure rotor and low pressure rotor. But distances between adjacent side frequencies of intershaft bearing keep constant and are equal to F_{interb} under different rotation speeds of high pressure rotor and low pressure rotor. The characteristic of intershaft bearing fault information in RSDD frequency spectrum is called "constant distances".

Rewriting (4), RSDD envelop spectrum is obtained,

$$\hat{X}(\omega') = \sum_{k=1}^{M} \hat{A}_{\mathrm{hb}k}\left(kF_{\mathrm{hb}}\frac{1}{1-\eta}\right)e^{j\beta_{\mathrm{hb}k}}\delta\left(\omega' - kF_{\mathrm{hb}}\frac{1}{1-\eta}\right)$$

$$+ \sum_{k=1}^{S} \hat{A}_{\mathrm{lb}k}\left(kF_{\mathrm{lb}}\frac{\eta}{1-\eta}\right)e^{j\beta_{\mathrm{lb}k}}\delta\left(\omega' - kF_{\mathrm{lb}}\frac{\eta}{1-\eta}\right) \quad ,$$

$$+ \sum_{k=1}^{P} \hat{A}_{\mathrm{interb}k}\left(kF_{\mathrm{interb}}\right)e^{j\beta_{\mathrm{interb}k}}\delta\left(\omega' - kF_{\mathrm{interb}}\right)$$

(8)

Equation (8) shows that, different from other bearings, the fault response of intershaft bearing keeps its position constant on RSDD envelop spectrum, and its characteristic frequencies are equal to $\omega' = kF_{\mathrm{interb}}$. The characteristic of intershaft bearing fault information in RSDD envelop spectrum is called "constant frequencies".

Characteristics of "constant distances" and "constant frequencies" can be used to diagnose fault of intershaft bearing.

III. CHARACTERISTIC DEFECT MULTIPLE FREQUENCIES OF INTERSHAFT BEARING

For a bearing with a stationary outer race, the characteristic defect multiple frequencies are defined as the ratios of characteristic defect frequencies to shaft rotation speed [2,3,4]. In this paper, the characteristic defect multiple frequencies of intershaft bearing are defined as the ratios of characteristic defect frequencies to the difference between outer race rotation speed and inner race rotation speed [5,6,7]. The characteristic defect multiple frequencies of intershaft bearing are expressed by the following equations[8,9,10]:

inner race defect multiple frequency,

$$F_{\mathrm{i}} = \frac{f_{\mathrm{i}} \times 60}{|n_{\mathrm{i}} - n_{\mathrm{e}}|} = \frac{1}{2}\left(1 + \frac{d\cos\alpha}{D_{\mathrm{m}}}\right)z , \qquad (9)$$

outer race defect multiple frequency,

$$F_{\mathrm{e}} = \frac{f_{\mathrm{e}} \times 60}{|n_{\mathrm{i}} - n_{\mathrm{e}}|} = \frac{1}{2}\left(1 - \frac{d\cos\alpha}{D_{\mathrm{m}}}\right)z , \qquad (10)$$

rolling element defect multiple frequency,

$$F_{\mathrm{b}} = \frac{f_{\mathrm{b}} \times 60}{|n_{\mathrm{i}} - n_{\mathrm{e}}|} = \frac{D_{\mathrm{m}}}{d}\left(1 - \frac{d^2}{D_{\mathrm{m}}^2}\cos^2\alpha\right) , \qquad (11)$$

where f_{i}, f_{e} and f_{b} are characteristic defect frequencies of inner race, outer race and rolling element, n_{i} and n_{e} are rotation speed of inner race and outer race, d is the diameter of rolling element, α is the contact angle, D_{m} is the pitch diameter, z is the number of rolling elements.

Generally, n_i and n_e a certain intershaft bearing are Ω_l and Ω_h of the aero engine.

IV. EXPERIMENTAL RESULTS

A. Experimental Setup

The experimental setup is shown in Fig.1. High pressure rotor is driven by high pressure motor when low pressure rotor is driven by low pressure motor. One end of high pressure rotor is supported on squirrel cage flexible support, and the other end is supported on outer race of intershaft bearing. The inner race of intershaft bearing is supported on low pressure motor. The intershaft bearing is lubricated by lubricating oil. Lubricating oil is ejected by oil pump into raceway of intershaft bearing via sucker and nozzle, and return to the oil pump via oil return pipe oil catch ring.

Rotation speeds of high pressure rotor and low pressure rotor are measured by Schenck P-84 photoelectric sensor and reflector paper. Acceleration vibration signal is measured by Schenck AS-020 piezoelectric sensor which is installed on support bearing housing (see Fig.1.10). The radial displacement of disk is measured by Schenck IN-085 eddy current displacement sensor.

1024 vibration data are collected at every $T = \dfrac{1}{\Omega_h - \Omega_l}$. A group of data contains data of continuous $32T$.

Photo of intershaft bearing is shown in Fig.2. Fig.3 shows the local fatigue peeling outer race of the intershaft bearing. The intershaft bearing is a single row cylindrical rolling bearing. Its geometric parameters are shown in Table 1. Its characteristic defect multiple frequencies are shown in Table 2. The intershaft bearing has local spalling on its outer raceway.
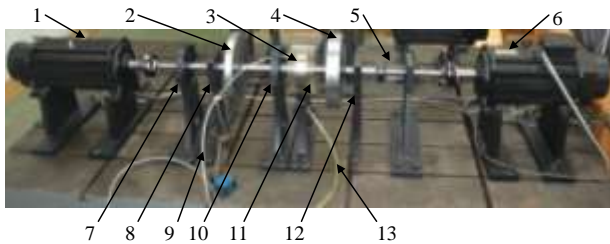
1. low pressure motor; 2. low pressure rotor disk; 3. intershaft bearing housing; 4. high pressure rotor disk; 5. squirrel cage flexible support; 6. low pressure motor; 7. support bearing housing of low pressure rotor; 8. vibration limiter; 9. sucker; 10. support bearing housing of low pressure rotor; 11. oil catch ring; 12. vibration limiter; 13. oil return pipe
Figure 1. Intershaft bearing test rig

Figure 2. Photo of intershaft bearing

Figure 3. Photo of local fatigue peeling outer race of intershaft bearing

Table 1 Geometric parameters list of intershaft bearing

diameter of the rolling element d(mm)	pitch diameter D_m(mm)	contact angle α (°)	number of rolling elements z
8	125	0	34

Table 2 Characteristic defect multiple frequencies of intershaft bearing

outer race defect F_e	inner race defect F_i	Rolling element defect F_b
15.912	18.088	15.561

B. Analysis of Defect Intershaft Bearing Vibration

Fig.4 shows vibration wave of signal collected from accelerometer under outer race rotation speed 1200 rpm and inner race rotation speed 300 rpm. Fig.5 and Fig.6 show frequency spectrum and envelop spectrum of the signal in RSDD. In Fig.4, abscissa axis represents RSDD period T, $1T = \dfrac{1}{\Omega_h - \Omega_l}$. In Fig.4 and Fig.5, abscissa axis represents RSDD frequency ω', $\omega' = \dfrac{\omega}{\Omega_h - \Omega_l}$, where ω is ordinary frequency. And $1X = \Omega_h - \Omega_l$.

Fig.4 shows that, vibration wave is not of obvious periodicity. Fig.5 shows that, in RSDD vibration spectrum, resonance area is in high frequency band. There are adjacent side frequencies, the distance between which is equal to F_e. Fig.6 shows that, in RSDD envelop spectrum, the amplitude of frequency F_e is biggest. Fig.7 and Fig.8 show frequency spectrum and envelop spectrum in RSDD under outer race rotation speed 900 rpm and inner race rotation speed 300 rpm. because of the decrease of relative rotation speed, amplitudes in Fig.5 and Fig.6 are smaller than amplitudes in Fig.5 and Fig.6 as a whole. In Fig.7, in high frequency band, there are adjacent side frequencies between which the distance is equal to F_e, which is the same as in Fig.5. It is proved that frequency spectrum in RSDD is of characteristic "constant distances". The same as in Fig.6, the amplitude of frequency F_e is biggish in RSDD envelop spectrum in Fig.8, which proves that envelop spectrum in RSDD is of characteristic "constant frequencies".

Fig.4 to Fig.8 show that, vibration signal measured from support bearing housing near the intershaft bearing is of characteristic "constant distances" as well as "constant frequencies", which proves that the theory of (7) and (8) is right.

It is need to point out that, characteristic "constant frequencies" almost appears in every group of experimental data when characteristic "constant distances" often appears.
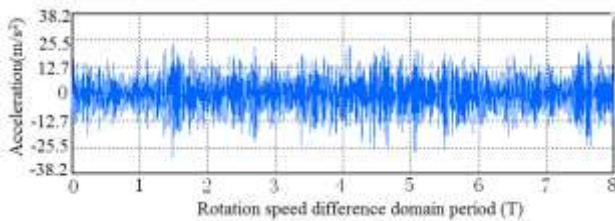
Figure 4. Vibration wave of intershaft bearing
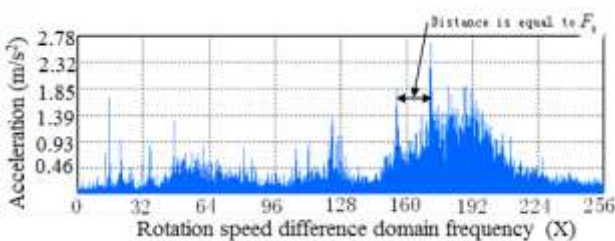
Figure 5. Vibration spectrum in RSDD of intershaft bearing
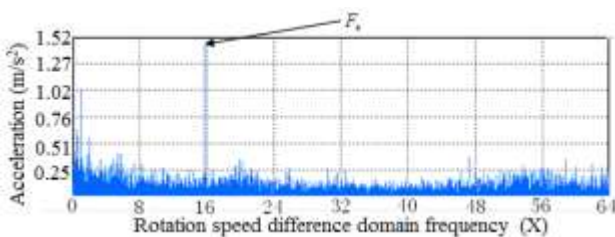
Figure 6. Vibration envelope spectrum in RSDD of intershaft bearing
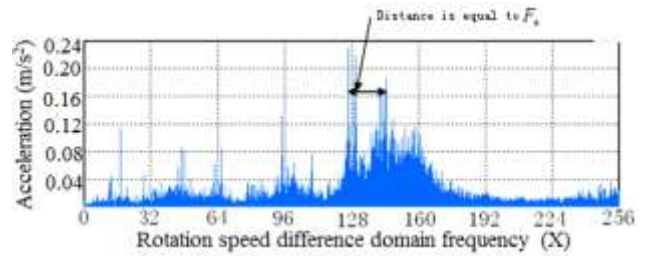
Figure 7. Vibration spectrum in RSDD of intershaft bearing
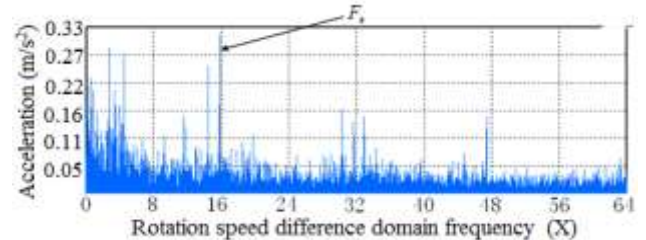
Figure 8. Vibration envelope spectrum in RSDD of intershaft bearing

C. Analysis of Rotor Unbalance and Misalignment Signal.

Since frequencies of unbalance response and misalignment response in this experiment are in low frequency band and accelerometer is not suitable for measure low frequency signal, eddy current displacement sensor is used to measure unbalance response and misalignment response. Fig.9 is vibration displacement signal wave of low pressure disk. Fig.9 (a) is the wave under high pressure rotation speed 900 rpm and low pressure rotation speed 300 rpm. Fig.9 (b) is the wave under high pressure rotation speed 1200 rpm and low pressure rotation speed 300 rpm. Fig.10 is frequency spectrum of low pressure disk displacement in RSDD. Fig.10 (a) is the spectrum under high pressure rotation speed 900 rpm and low pressure rotation speed 300 rpm. Fig.10 (b) is the spectrum under high pressure rotation speed 1200 rpm and low pressure rotation speed 300 rpm.

Fig.10 shows that, in RSDD frequency spectrum, positions of frequencies caused by unbalance response and misalignment response and distances between these frequencies change along with the difference between high pressure rotation speed and low pressure rotation speed. It is proved that unbalance response and misalignment response are not of characteristics "constant distances" and "constant frequencies", which is consistent with theory of (7) and (8).
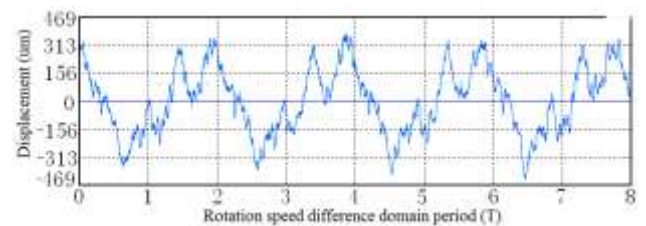
(a).High pressure rotor rotation speed is 900 rpm, low pressure rotor rotation speed is 300 rpm
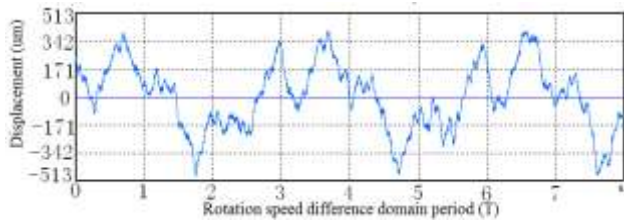
(b).High pressure rotor rotation speed is 1200 rpm, low pressure rotor rotation speed is 300 rpm

Figure 9. Vibration displacement signal wave of low pressure disk
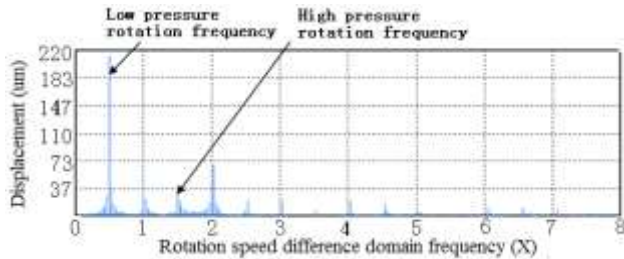
(a).High pressure rotor rotation speed is 900 rpm, low pressure rotor rotation speed is 300 rpm
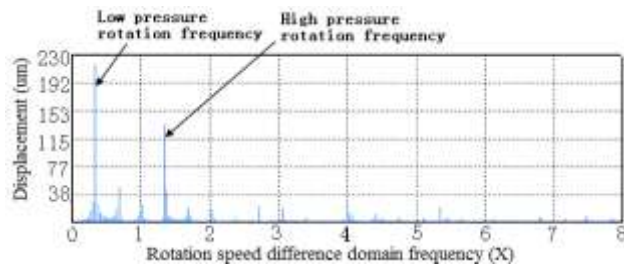
(b).High pressure rotor rotation speed is 1200 rpm, low pressure rotor rotation speed is 300 rpm

Figure 10. Spectrum of low pressure disk displacement in RSDD

V.   CONCLUSIONS

Under variational rotation speeds of outer race and inner race, in RSDD frequency spectrum of intershaft bearing with fault, side frequencies appear in high frequency band, between which the distances keep constant. This characteristic is called "constant distances".

Under variational rotation speeds of outer race and inner race, in RSDD envelop spectrum of intershaft bearing with fault, the characteristic defect multiple frequencies of intershaft bearing keep their positions constant. This characteristic is called "constant frequencies".

Unbalance response, misalignment response, and defect vibration of bearings with a stationary race are not of these characteristics.

The experimental results indicate that, vibration of intershaft bearing with a fault is of characteristic "constant distances" and "constant frequencies".

REFERENCES

[1]   Lei Jianyu and Liao Mingfu, "Extracting Feature Information and its Visualization Based on the Characteristic Defect Octave Frequencies in a Rolling Element Bearing," Data Science Journal 6 (2007): 596-602.

[2]   LEI Jianyu, LIAO Mingfu, "A New Approach Based on the Defect Characteristic Octave Frequncies to Diagnose Local Defects in a Rolling Element Bearing," Measurement & Control Technology, Year 2007, Issue 9, Page 72-75. (in Chinese)

[3]   MENG Tao, LIAO Mingfu, "Detection and diagnosis of the rollimg element bearing fault by the delayed correlation envelope technique," Acta Aeronautica et Astronautica Sinica, 2004, 25(1): 41-44. (in Chinese)

[4]   LEI Jianyu, Vibration Analysis and Diagnosis on the Local Fault of a Rolling Element Bearing [D]. (in Chinese)

[5]   Zhao Mingbo, Jin Xiaohang, Zhang Zhao, Li Bing, "Fault diagnosis of rolling element bearings via discriminative subspace learning: visualization and classification," EXPERT SYSTEMS WITH APPLICATIONS, 2014,41(7): 3391-3401.

[6]   Liu Huanhuan, Han Minghong, "A fault diagnosis method based on local mean decomposition and multi-scale entropy for roller bearings" MECHANISM AND MACHINE THEORY, 2014, Issue 75: 67-78.

[7]   Gur Sourav, Mishra Sudib K, Chakraborty, Subrata "Performance assessment of buildings isolated by shape-memory-alloy rubber bearing: Comparison with elastomeric bearing under near-fault earthquakes," STRUCTURAL CONTROL & HEALTH MONITORING, 2014,21(4): 449-465.

[8]   Jena DP., Panigrahi SN, Zhang Zhao, Li Bing, "Motor bike piston-bore fault identification from engine noise signature analysis," APPLIED ACOUSTICS, 2014, Issue 76: 35-47.

[9]   Georgoulas G, Loutas, T, Stylios, CD, Kostopoulos, V, "Bearing fault detection based on hybrid ensemble detector and empirical mode decomposition," MECHANICAL SYSTEMS AND SIGNAL PROCESSING, 2014,41(1-2): 510-525.

[10]   Tesei T, Collettini C, Viti C, Barchi MR, "Fault architecture and deformation mechanisms in exhumed analogues of seismogenic carbonate-bearing thrusts," JOURNAL OF STRUCTURAL GEOLOGY, 2014, Issue 55: 167-181.